Effect of the Endosomal Acidification on Small Ion Transport through the Anthrax Toxin PA_{63} Channel

Nnanya Kalu[1], Antonio Alcaraz[2], Goli Yamini[1], Sanaz Momben Abolfath[1], Laura Lucas[1], Clare Kenney[1], Vicente M. Aguilella[2], Ekaterina M. Nestorovich[1]*

[1]Department of Biology, The Catholic University of America, 620 Michigan Ave, Washington, DC, USA, 20064
[2]Laboratory of Molecular Biophysics, Department of Physics, Universitat Jaume I, 12071 Castellón, Spain

*Corresponding author
Fax: 202-319-5271
Tel: 202-319-6723
E-mail address: Nestorovich@cua.edu

Abstract

Tight regulation of pH is critical for the structure and function of cells and organelles. The pH environment changes dramatically along the endocytic pathway, an internalization transport process that is 'hijacked' by many intracellularly active bacterial exotoxins, including the anthrax toxin. Here we investigate the role of pH on single-channel properties of the anthrax toxin channel, PA_{63}. Using conductance and current noise analysis, blocker binding, ion selectivity, and PEG partitioning measurements, we show that the channel exists in two different open states (*'maximum'* and *'main'*) at pH ≥ 5.5, while only a maximum conductance state is detected at pH < 5.5. We describe two substantially distinct patterns of PA_{63} conductance dependence on KCl concentration uncovered at pH 6.5 and 4.5.

Keywords:

Access resistance, *Bacillus anthracis*, current fluctuations, endosomal acidification, multi-state conductance

Introduction

A number of the so-called '*unconventional'* ion channels [1] operate under harsh or asymmetrical pH conditions. One of the most prominent examples is bacterial porins, which are able to function under acid stress conditions of the stomach and severe pH gradient across bacterial outer membranes. Many aspects of the pH-dependent behavior of bacterial porins have been investigated using single-molecule experiments with *Escherichia coli* outer membrane protein F in bilayer lipid membranes [2-6]. Another striking example relates to bacterial binary AB type exotoxins, where the B components not only specifically form channels under low endosomal pH but have also evolved to transport their A components into the cytosol, making use of endosomal membrane pH gradients. In this study, we investigate the effect of the endosomal acidification on small-ion transport through the channel-forming B component of the anthrax toxin, which is secreted by the virulent strains of *Bacillus anthracis*.

Host cell entry of the anthrax toxin is attained through clathrin-mediated [7] endocytosis [8] (Fig. 1). The anthrax toxin consists of three proteins, two A components, lethal factor (LF) and edema factor (EF), and one B

component, protective antigen (PA). LF and EF are intracellularly active enzymes that bind to the receptor-bound PA to enter the host cell. The anthrax toxin uptake occurs in several stages (see Fig. 1 legend for detail). Briefly, 83 kDa protective antigen (PA_{83}), binds to specific cellular TEM8 [9] and CMG2 [10] receptors [11-15] and, after being cleaved by a furin-like protease [16] into PA_{63}, self-assembles to form a ring-shaped heptameric/octameric prepore that can simultaneously bind three (in heptamer) [17] or four (in octamer) [18] molecules of LF and/or EF. The complex is then endocytosed [19] and, under acidic conditions of the endosome, the prepore converts to a transmembrane pore. The formed channel is then believed to work as an effective translocase, capable of unfolding and translocating LF and EF into the cytosol under a pH gradient across the late endosomal limiting [20, 21] and intraluminal vesicle [22, 23] membranes. An alternative anthrax toxin uptake model suggests that the toxin delivers its enzymatic cargo by catalyzing the rupture of the limiting endosomal membranes [24].

PA_{63} is an extended 180-Å long "flower-on-a-stem" 14-strand β-barrel [25] channel with a 75-Å-long bud and a 105-Å-long stem and radius varying from ~ 3 to 16 Å [26]. The pH dependence of the channel-mediated LF uptake (binding and translocation) has been extensively studied *in vitro* using the planar lipid bilayer technique [27], where the anthrax toxin channels cleaved to PA_{63} were shown to spontaneously form stable highly cation-selective voltage-gated channels [28]. The channel has an approximately ohmic and small conductance (85-110 pS in 0.1 M KCl, pH 6.6), compared to the other β-barrel channels [29]. Conductance values as low as 55 pS (0.1 M KCl, pH 5.5) [30] and alternate conductance states of open PA_{63} [29, 31, 32] were also reported. The unusually low conductivity of the channel was explained by the presence of a steric bottleneck [33], composed of a narrow ring of the hydrophobic phenylalanine (Phe^{427}) side chains (the so called ϕ-clamp) located at the junction of the bud with the stem region [30]. Interestingly, PA_{63} channel conductance was reported to be only weakly dependent on salt concentration between 10 and 200 mM KCl [29]. This finding was explained by charge effects of the negatively charged groups in the channel lumen resulting in the generation of a considerable ionic strength dependent potential that attracts cations and repels anions [34]. To our surprise, despite the high importance and relative simplicity of the tacit experiments, the influence of solution pH on the PA_{63} channel properties *per se* was not investigated, apparently because of an incorrect assumption that these properties are not altered. Given the important role of pH change in the anthrax toxin internalization process, the current study is designed to address the disparity.

Material and Methods

PA_{63} was purchased from List Biological Laboratories, Inc. (Campbell, CA). The following chemical reagents were used: KCl, MES, KOH, HCl, PEG 400 (Sigma-Aldrich, USA); methyltriphenylphosphonium chloride (MTPP), "purum" hexadecane (Fluka, Buchs, Switzerland); diphytanoyl phosphatidylcholine, DPhPC (Avanti Polar lipids, Inc., Alabaster, AL); pentane (Burdick and Jackson, Muskegon, MI), agarose (Bethesda Research Laboratory, Gaithersburg, MD). Per-6-(3-aminopropylthio)-β-cyclodextrin (AmPrβCD) was a kind gift of Dr. Vladimir Karginov, KFBio, LLC. Milli-Q water was used to prepare solutions.

The single-channel bilayer cell was custom-made with a two-compartment (*cis* and *trans*) Teflon chamber separated by a 15-μm-thick Teflon partition with ~ 60-80 μm diameter aperture for bilayer membrane formation. 1.5 ml of 0.01 – 3 M KCl solutions was added to both *cis* and *trans* sides of the chamber symmetrically. KCl: 0.5 M *cis* | 1 M *trans*, 0.1 M *cis* | 0.5 M *trans*, 0.01 M *cis* | 0.05 M *trans*, and reversed gradients were used for the selectivity measurements. To form "solvent-free" planar lipid bilayers with the lipid monolayer opposition technique [35], we added 10 μl of 5 mg/ml stock solution of DPhPC in pentane to *cis* and *trans* sides of the bilayer chamber. The 0.01 - 3 M aqueous solutions of KCl were buffered at pH 4 – 7.5 (5 mM MES) at room temperature (23 ± 0.5)°C. Single channels were formed by adding 1-2 μl of 20 μg ml^{-1} solution of PA_{63} to the 1.5 ml aqueous phase on the *cis* half of the chamber after bilayer formation. Under this protocol, the channel insertions were always directional as judged by the asymmetry of PA_{63} voltage gating [28]. The electrical potential difference (V = + 50 and + 100 mV) across the membrane was applied and current signal was recorded with a pair of Ag-AgCl electrodes in 2 M KCl, 1.5% agarose bridges assembled within standard 200 μl pipette tips. The applied potential was defined as positive if it was higher on the side of PA_{63} addition (*cis* side). The current was amplified by an Axopatch 200B amplifier (Molecular Devices, LLC) in the voltage clamp mode (whole cell β = 1) with a CV-203BU headstage. Data were digitized with Digidata 1440A while the output signal was filtered by a low-pass 8-pole Butterworth filter (Model 900, Frequency Devices Inc.), at 15 kHz and directly saved into the computer memory with a sampling frequency of 50 kHz. Current amplitude analysis was performed using ClampFit 10.6 software. The membrane chamber and headstage were isolated from external noise sources with a double μ-metal Faraday cage (custom ordered from Amuneal Manufacturing Corp.). Depending on PA_{63} activity, 30 – 200 single channel events were analyzed for the conductance measurements. The reversal potential data were averaged over 6 – 10 separate measurements. Values are given as the means ± SD. The Student's t-test (StatDisk 13, Triola Stats) was used to compare the means.

Results and Discussion

The 'maximum' and 'main' conductance states of the open PA_{63} channel

PA_{63} channel-forming activity is known to be pH-dependent requiring mildly acidic pH for the channels to form. Using the monolayer opposition technique, we were able to successfully reconstitute stable PA_{63} channels (Fig. 2) in *cis*|*trans* symmetrical 1 M (Fig. 2A and 2B) and 0.1 M KCl (Fig. 2C) solutions with pH ranging from 7.5 (Fig. 2A, top) to 4 (Fig. 2A, bottom). In accordance with the earlier report [28], the channel-forming activity of PA_{63} was increased in sub-acidic (pH 5 – 6.5) solutions, and decreased in neutral (pH 7-7.5) and acidic (pH ≤ 4.5) solutions. Under the described conditions, the formed PA_{63} channels were exclusively heptameric (see Fig. S3 in ref. [36]). At pH ≥ 5.5, two PA_{63} conductance states, mentioned [29] and described [31] earlier, were frequently detected (labeled as conductance state '*max*' and '*main'* in Fig. 2). The channels are often seen inserting into the maximum conductance state and quickly (≤ secs) changing to the main conductance state. The maximum

conductance state can then reappear, as seen at the pH 6.5 single PA_{63} current recording (Fig. 2B, top). At pH 6.5, the ratio between the maximum and main state conductances was greater in 1 M (Fig. 2B, top) compared to 0.1 M KCl (Fig. 2C, top) solutions, (27 ± 4) % and (11 ± 1) % respectively.

The alternate conductance states of open PA_{63} channels were recently rediscovered by Das and Krantz [32] (see discussion in refs [37, 38]). To provide support for the allosteric helix compression model of LF translocation through PA_{63} [39], the authors hypothesize that the two conductance states of PA_{63} represent the so-called 'clamped empty' and 'unclamped empty dilated' states of the channel, with the dilation occurring at the ϕ-clamp. While this conclusion was made based on the Monod, Wyman, and Changeux allostery model fit applied to data on the PA_{63} ion current blockage by LF peptides, no direct statistical comparison of the peptide binding in the maximum and main conductance states was offered. To test whether the maximum and main conductance states correspond to the two structurally distinct conformations of the channel, we studied partitioning of a water-soluble polymer, polyethyleneglycol, with a molecular weight of 400 Da (PEG 400), into the channel lumen at pH 6.5 (Fig. 3A). Previously, the polymer partitioning technique [40] was effectively used as a tool to size the functional states of ion channel structures, including PA_{63} [41]. PEG 400 was chosen because this polymer was shown to cause the most significant PA_{63} current reduction [41] and therefore is expected to be sensitive to the potential changes in the PA_{63} channel dimensions. PEG-induced current decrease has some detectable but very small difference (p-value = 0.003) when compared for the maximum and main conductance states of the channel. Thus $\frac{G_{\mathrm{PEG}}}{G_{\mathrm{no\ PEG}}}$ conductance ratio was equal to 0.24 ± 0.02 for the maximum state and 0.2 ± 0.01 for the main state.

In addition, the potential structural changes, which PA_{63} channel may undergo when switching from the maximum to main conductance state, do not appear to be significant enough to alter the ion selectivity of the channel (Fig. 3B). Thus, in both the maximum and main conductance states, the channel shows ~3 times higher preference for cations compared to anions (compare $E_{\mathrm{rev}} = 9.1 \pm 0.5$ mV and 8.6 ± 0.4 mV for the maximum and main conductance states, respectively). Note that the lower cation selectivity value compared to ones previously reported [28] is due to the high salt concentrations used to perform the measurements. The high, 0.5 M *cis* | 1 M *trans*, KCl concentration gradient was used for the reversal potential measurements because of the higher difference between the maximum and main state conductances observed at high KCl concentrations (compare Fig. 2B and C). Moreover, kinetic parameters of the PA_{63} channel inhibition (Fig. 3C) by the high-affinity 7+β-cyclodextrin channel blocker (AmPrβCD, Fig. 3D, left) [42], examined using the power spectral density analysis (Fig. 3E), are nearly identical for the main and maximum conductance states. In both states, the AmPrβCD-induced current fluctuations can be described as a two-state Markov process, manifested by an approximately Lorentzian shape of the power spectral density. The AmPrβCD/PA_{63} binding reaction kinetic parameters, calculated as described in ref. [31] for the same single PA_{63} channel, were within the limit of experimental error: $t_{\mathrm{off}}^{\mathrm{max}} = (98 \pm 2)$ ms *vs.* $t_{\mathrm{off}}^{\mathrm{main}} = (93 \pm 3)$ ms and $k_{\mathrm{on}}^{\mathrm{max}} = (2.23 \pm 0.07) \times 10^7\ (\mathrm{M\ s})^{-1}$ *vs.* $k_{\mathrm{on}}^{\mathrm{main}} = (2.38 \pm 0.05) \times 10^7\ (\mathrm{M\ s})^{-1}$. Some may argue that even though AmPrβCD was previously shown to interact with the Phe^{427} residue [43], the blocker is too large to enter and, therefore, to probe the potential ϕ-clamp dilation. To

clarify this issue, we performed a similar experiment (Fig. 3F) with a potent small-molecule PA_{63} blocker, methyltriphenylphosphonium ion (MTPP) (Fig. 3D, right), that not only was suggested to bind to Phe^{427} [30], but is also small enough to translocate (Fig. 3G) through the binding site region. Both the residence time and, importantly, size-dependent on-rate of the MTPP/PA_{63} binding reaction were: $t_{\mathrm{off}}^{\mathrm{max}} = (8.97 \pm 0.02)$ ms *vs.* $t_{\mathrm{off}}^{\mathrm{main}} = (9.01 \pm 0.03)$ ms and $k_{\mathrm{on}}^{\mathrm{max}} = (1.11 \pm 0.03) \times 10^8$ $(\mathrm{M\ s})^{-1}$ *vs.* $k_{\mathrm{on}}^{\mathrm{main}} = (1.14 \pm 0.04) \times 10^8$ $(\mathrm{M\ s})^{-1}$ when measured for the same single PA_{63} channel. Therefore, if indeed the main to maximum state transformation represents PA_{63} channel dilation at the ϕ-clamp region, as claimed by the ref. [32] authors, it is unclear why both AmPrβCD and MTPP blockers are not sensitive to these structural changes. In addition, at pH > 5.5 PA_{63} channels were frequently recorded being inserted in the maximum conductance state (see Fig. 3A in ref. [31]), without switching to the main conductance state, similar to the described PA_{63} current recordings at pH 4.5 (Fig. 2B and C, bottom tracks).

To conclude this section, we emphasize that, even under conditions where the two-conductance-state behavior was most evident (1 M KCl, pH > 5.5), we did not observe any significant difference between the channel's functional properties in these two states. Indeed, the parameters of both the small ion selectivity (Fig. 3B) and AmPrβCD and MTPP blocker binding (Figs. 3E and 3F) were nearly identical, while the PEG partitioning experiments (Fig. 3A) indicated only a minor change in the overall channel dimensions.

PA_{63} conductance changes with solution pH

Driven by a relatively high discrepancy between the earlier reported single PA_{63} conductance data (from 55 to 100 pS in 0.1 M KCl), we measured ionic current through the channel in the narrow 4 – 7.5 pH range available for such experiments (Fig. 4A). Note that pH dependence of the PA_{63} single-channel current has the following four distinctive features. ***(1)*** Not only do the two alternate conductance states appear at pH ≥ 5.5 [32], but the difference between the states becomes smaller with lowering pH from 7.5 to 6 and nearly vanishes at pH 5.5. Moreover from the analysis of the monotonic conductance change with pH, it appears that at pH < 5.5, the channels insert and remain in the maximum conductance state without switching to the main conductance state (*filled symbols*). Additional evidence supporting this conclusion comes from the power spectrum analysis of the PA_{63} current fluctuation (Fig. 4B). At pH 6.5, power spectrum of the current fluctuation in the main conductance state (*green spectra* in Fig. 4B) has an additional high frequency component at 100 – 1200 Hz, which reflects the more intense fluctuations of the open channel current when in the main conductance state (compare parts of the same single ion channel current recording marked in *green* and *red* in Fig. 2B). At the same time, in the power spectrum of the PA_{63} current at pH 4.5 (*violet spectra in Fig. 4B*) the high frequency component is absent. The spectrum shows an ideal *1/f*-type behavior, just as in the maximum conductance state at pH 6.5 (*red spectra in Fig. 4B*), at a wide 3-1000 Hz range of frequencies. ***(2)*** PA_{63} current monotonically decreases with solution pH when the channel is in the maximum conductance state. The effect, that is most likely due to reversible protonation/deprotonation of the charged residues in the channel lumen, is more significant in low salt

concentration; ~ 3.4 times in 0.1 M KCl *versus* ~ 1.2 times in 1 M KCl. ***(3)*** PA_{63} conductance increase, when switching from 0.1 M KCl to 1 M KCl, is more significant at low pH compared to higher pH. Thus we observed ~ 5 times increase in PA_{63} current at pH 4.5 compared to only 2-times increase at pH 6.5 (marked by the two vertical dashed lines in Fig. 4A). ***(4)*** If both main and maximum conductance states of the open channel are included, PA_{63} single-channel conductance varies from 27 ± 1 to 90 ± 16 pS in 0.1 M KCl and 125 ± 5 to 190 ± 10 pS in 1 M KCl, at 4 – 7.5 pH range. This finding can explain the wide discrepancy of the earlier reported PA_{63} conductance values.

Solution pH and two distinct patterns of PA_{63} conductance dependence on KCl concentration

To further investigate pH influence on the PA_{63} conductance/KCl concentration relationship, we tested PA_{63} single-channel current over a wide (0.01 – 3 M) range of KCl concentrations, separately at pH 4.5 and pH 6.5 (Fig. 5A). Interestingly, while at pH 6.5 both maximum and main conductance states (*circles*) follow the earlier described [29, 34] weak concentration behavior; they display linear, close to 1:1, dependence on the KCl solution conductivity at pH 4.5 (*squares*). This finding indicates that one or several amino acid residues with ionizable side chains in the channel lumen, that create the ionic strength-dependent potential contributing to the strong cation selectivity of the channel [34], and apparently K^+ binding, change their ionization state with lowering solution pH. At the same time, the 1:1 dependence of ion channel conductance on bulk solution conductivity is expected for a neutral non-selective pore [44, 45], which is obviously not the case in this system. Even though in high KCl concentrations, we observed a moderate decrease in the cationic selectivity of the channel when lowering solution pH (Fig. 5B, top) (as predicted in ref. [33]), PA_{63} still demonstrates a strong preference for cations at pH 4.5. Thus using 0.1 M *cis* | 0.5 M *trans* KCl solution gradient, we found reversal potential $E_{\mathrm{rev}} = 33.3 \pm 0.9$ mV and 27.0 ± 0.8 mV at pH 6.5 and pH 4.5, respectively. Similarly, in 0.01 M *cis* | 0.05 M *trans* KCl solution gradient (Fig. 5B, bottom) the reversal potential $E_{\mathrm{rev}} = 28.8 \pm 1.0$ mV and 33.7 ± 2.7 mV at pH 6.5 and pH 4.5 respectively. At the same time, the common observation in protein channels with ionizable residues, that determine their ion-selective properties, is conductance saturation at low enough bulk concentration, i.e. under conditions when ion concentrations within the pore are imposed by the channel charges and the requirement of electroneutrality [45]. An explanation for the observed PA_{63} conductance behavior may come from analysis of the different factors contributing to the total channel conductance. For that we need to account for the complex interplay of the ionizable amino acid residues in the channel lumen and the steric constriction created by the narrow region formed by the ϕ-clamp. It is well appreciated that access resistance to a channel aperture may become a significant part of the total, measured, channel resistance at low salt concentration [46, 47]. Note that here we refer to the access resistance from the channel cavity to the narrow bottleneck and not to the interface between bulk solution and the channel mouth. In addition, access resistance scales inversely with local solution conductivity [48] which in the present case is considerably smaller than the one in bulk due to hydrophobic effects [30]. We suggest that at pH 6.5 a ring of charged residues (possibly His211 with pKa ~5.8 or Asp231 with pKa

~5.7) at the entrance of the channel bottleneck region induce ion accumulation lowering the access resistance contribution. The pKa values were calculated using the PA_{63} structure (PDB code 3J9C) and PROPKA3.0 software in the PDB2PQR server [49]. In contrast, at pH 4.5 the cavity residues are protonated and ion excess faints. The PA_{63} conductance is then determined by the access resistance [46, 50, 51] to the bottleneck ϕ-clamp region of the channel. One may wonder why the protonation of the cavity residues does not appreciably change channel selectivity (Fig. 5B). To answer this question, note that channel conductance is often determined by the narrowest part of the channel and the ionizable residues in it, whereas selectivity is the result of the concerted action of many residues [52], some of them even buried in the protein [53]. In addition, the small asymmetry in reversal potential seen when reversing the concentration gradient (Fig. 5B) may also be an indication that the charged residues responsible for channel selectivity are not located near one of the channel entrances. This hypothesis is supported by calculations performed by Lee et al. [33] showing that the protonation of several histidine residues dramatically changes the electric potential drop, mainly in the bottleneck of the channel (Fig 9 in ref. [33]).

Concluding Remarks

In this article, we examined small ion transport properties of the anthrax toxin channel in the physiologically relevant range of solution pH (4 – 7.5). Even though the PA_{63} channel ability to bind and translocate the enzymatic LF and EF proteins has been investigated in a number of studies, pH-dependent behavior of the channel *per se* has so far remained largely unexplored. The major findings of this work are as follows:

1. The relatively wide discrepancy between the reported single PA_{63} channel conductance data are determined by two factors. First, PA_{63} maximum conductance gradually decreases with lowering solution pH, from 7.5 to 4 (Fig. 4A). The effect is more significant in 0.1 M compared to 1 M KCl solutions. Second, at pH ≥ 5.5, the earlier described [31] '*maximum*' and '*main*' PA_{63} conductance states were frequently detected (Figs. 2B). If both conductance states are considered, PA_{63} channel conductance varies from 27 ± 1 to 90 ± 16 pS in 0.1 M KCl and 125 ± 5 to 190 ± 10 pS in 1 M KCl, at the investigated pH range.

2. While at pH > 5.5 two conductance states of the open PA_{63} are clearly detected, at acidic pH the channel inserts into the maximum conductance state as confirmed by the power spectral analysis of the current fluctuations (Fig. 4B). Ion selectivity (Fig. 3B) and blocker binding (Figs. 3E and F) in these two states are identical, whereas PEG partitioning experiments, which are not themselves free of the limitations discussed in ref. [41], detect only slight changes in the channel overall dimensions. In addition, if this effect does represent the dilation of the channel lumen at the ϕ-clamp region, important for the protein transport as suggested in ref. [32], it is unclear why the 'two-conductance-state' behavior is more prominent at pH ≥ 6.5 and high salt concentrations and why ~ 33 % of the channels at pH 6.6 were found to insert into the maximum conductance state without any change-over to the main state [31]. Considering the fact that at neutral pH (Fig. 2A), about 67% PA_{63} channels first insert into the maximum conductance state and quickly switch to the main conductance state, whereas at pH < 5.5 the channels

are always found in the maximum conductance state, we cannot rule out the possibility that the channel, evolved to operate in the acidic endosomal environment, at pH ≥ 5.5 forms but then collapses to the more energetically favorable but not fundamentally different conformation. These thoughts certainly cannot eliminate our eagerness to find out whether the cryo-EM structure of the channel [26] represents PA_{63} in its maximum or main conductance state.

3. The previously reported weak dependence of PA_{63} conductance on KCl concentration [29] is only observed at pH 6.5 but not at pH 4.5 where the channel conductance nearly scales with KCl solution conductivity (Fig. 5A). At the same time, lowering solution pH does not neutralize the channel, which still remains strongly cation selective (Fig. 5B). We believe that this behavior is determined by two different factors contributing to the total channel conductance. At pH 6.5, the major factor defining PA_{63} conductance is the fixed charges distribution in the channel lumen, namely one or several amino acid residues at proximity to the ϕ-clamp region that create ionic strength-dependent electrical potential that attracts cations. Taking into account the difference in PA_{63} conductance/KCl concentration relationship at pH 4.5, we suggest that K^+ ions inside the channel can either interact with the aromatic π-motif of the neutral forms of histidine residues *via* cation- π interactions [54] or bind to the negatively-charges glutamic or aspartic acid residues, provided their pKs in the channel lumen are shifted toward higher numbers (between 4.5 and 6.5). Thus, a considerable shift in pKs of a number of amino acids was previously predicted using Discovery Studio 2.0 and the theoretical model of the PA_{63} channel (PDB code 1V36) [24]. The same assumed binding can be responsible for the increased conductance values observed in high KCl concentrations (> 1 M) at pH 4.5 compared to pH 6.5 (Fig. 5A). At pH 4.5 when the putative residues get protonated, PA_{63} conductance at low KCl concentrations has a strong contribution from the access resistance of the narrow ϕ-clamp region of the channel. In our forthcoming publication, we plan to compute the access resistance of the small ion transport using PA_{63} WT and F427A mutant and further investigate the influence of the ionization state of the amino acid residues on the total conductance of the channel. In addition, we will examine small-ion transport properties of PA_{63} mimicking pH gradient conditions existing across late and early endosomal limiting and ILV membranes.

Author Contribution:

EMN conceived and supervised the study; NK, GY, AA, VMA, and EMN designed experiments; NK, GY, SMA, LL, CK, and EMN performed experiments; NK, AA, GY, SMA, VMA, and EMN analyzed and interpreted data; NK, AA, VMA and EMN wrote the manuscript; NK, AA, GY, SMA, LL, CK, VMA, and EMN made manuscript revisions.

Acknowledgements: We are very thankful to Dr. Vladimir Karginov, KFBio, LLC for providing AmPrβCD blocker. The project was financially supported by NIAID of the NIH under award number 1R15AI099897-01A1 and by The Catholic University startup funds (to Ekaterina Nestorovich). AA and VA acknowledge financial

support from the Spanish Government (FIS2013-40473-P and FIS2016-75257-P AEI/FEDER), and Universitat Jaume I (P1.1B2015-28). GY is supported by the American Dissertation Fellowship from AAUW.

Conflict of Interest: The authors declare no conflict of interest.

List of Abbreviations Used in the Article

PM	plasma membrane
RE	recycling endosome
EE	early endosome
MVB/ECV	multivesicular body/endosomal carrier vesicle
LE	late endosome
ILV	intraluminal vesicle
TEM8	tumor endothelial marker 8 receptor
CMG2	capillary morphogenesis gene 2 receptor
PA_{83}	protective antigen pre-pore
PA_{63}	protective antigen transmembrane pore
PA_{20}	protective antigen cleaved off
LF	lethal factor
EF	edema factor
PEG	polyethyleneglycol
V-ATPase	vacuolar-type H+-ATPase
AmPrβCD	per-6-(3-aminopropylthio)-β-cyclodextrin
MTPP	methyltriphenylphosphonium ion
MES	2-(*N*-morpholino)ethanesulfonic acid
OmpF	outer membrane protein F
DPhPC	diphytanoyl phosphatidylcholine
SD	standard deviation
E_{rev}	reversal potential
$t_{\mathrm{off}}^{\mathrm{max}}$	residence time of blocker/channel binding reaction measured at the maximum conductance state
$t_{\mathrm{off}}^{\mathrm{main}}$	residence time of blocker/channel binding reaction measured at the main conductance state
$k_{\mathrm{on}}^{\mathrm{max}}$	on-rate of blocker/channel binding reaction measured at the maximum conductance state
$k_{\mathrm{on}}^{\mathrm{main}}$	on-rate of blocker/channel binding reaction measured at the main conductance state
Phe	phenylalanine

References

1. Delcour AH (2015) *Electrophysiology of Unconventional Channels and Pores.* Springer International Publishing

2. Nestorovich EM, Rostovtseva TK, Bezrukov SM (2003) Residue ionization and ion transport through OmpF channels. Biophys J **85:** 3718-3729

3. Lopez ML, Queralt-Martin M, Alcaraz A (2016) Stochastic pumping of ions based on colored noise in bacterial channels under acidic stress. Nanoscale **8:** 13422-13428

4. Queralt-Martin M, Garcia-Gimenez E, Mafe S, Alcaraz A (2011) Divalent cations reduce the pH sensitivity of OmpF channel inducing the pK(a) shift of key acidic residues. Phys Chem Chem Phys **13:** 563-569

5. Alcaraz A, Queralt-Martin M, Verdia-Baguena C, Aguilella VM, Mafe S (2014) Entropy-enthalpy compensation at the single protein level: pH sensing in the bacterial channel OmpF. Nanoscale **6:** 15210-15215

6. Alcaraz A, Queralt-Martin M (2016) On the different sources of cooperativity in pH titrating sites of a membrane protein channel. Eur Phys J E Soft Matter **39:** 29

7. Abrami L, Liu S, Cosson P, Leppla SH, van der Goot FG (2003) Anthrax toxin triggers endocytosis of its receptor via a lipid raft-mediated clathrin-dependent process. J Cell Biol **160:** 321-328

8. Friedlander AM (1986) Macrophages are sensitive to anthrax lethal toxin through an acid-dependent process. J Biol Chem **261:** 7123-7126

9. Bradley KA, Mogridge J, Mourez M, Collier RJ, Young JA (2001) Identification of the cellular receptor for anthrax toxin. Nature **414:** 225-229

10. Scobie HM, Rainey GJ, Bradley KA, Young JA (2003) Human capillary morphogenesis protein 2 functions as an anthrax toxin receptor. Proc Natl Acad Sci U S A **100:** 5170-5174

11. Rainey GJ, Wigelsworth DJ, Ryan PL, Scobie HM, Collier RJ, Young JA (2005) Receptor-specific requirements for anthrax toxin delivery into cells. Proc Natl Acad Sci U S A **102:** 13278-13283

12. Wolfe JT, Krantz BA, Rainey GJ, Young JA, Collier RJ (2005) Whole-cell voltage clamp measurements of anthrax toxin pore current. J Biol Chem **280:** 39417-39422

13. van der Goot G, Young JA (2009) Receptors of anthrax toxin and cell entry. Mol Aspects Med **30:** 406-412

14. Liu S, Crown D, Miller-Randolph S, Moayeri M, Wang H, Hu H, Morley T, Leppla SH (2009) Capillary morphogenesis protein-2 is the major receptor mediating lethality of anthrax toxin in vivo. Proc Natl Acad Sci U S A **106:** 12424-12429

15. Wigelsworth DJ, Krantz BA, Christensen KA, Lacy DB, Juris SJ, Collier RJ (2004) Binding stoichiometry and kinetics of the interaction of a human anthrax toxin receptor, CMG2, with protective antigen. J Biol Chem **279:** 23349-23356

16. Molloy SS, Bresnahan PA, Leppla SH, Klimpel KR, Thomas G (1992) Human furin is a calcium-dependent serine endoprotease that recognizes the sequence Arg-X-X-Arg and efficiently cleaves anthrax toxin protective antigen. J Biol Chem **267:** 16396-16402

17. Mogridge J, Cunningham K, Collier RJ (2002) Stoichiometry of anthrax toxin complexes. Biochemistry **41:** 1079-1082

18. Kintzer AF, Thoren KL, Sterling HJ, Dong KC, Feld GK, Tang II, Zhang TT, Williams ER, Berger JM, Krantz BA (2009) The protective antigen component of anthrax toxin forms functional octameric complexes. J Mol Biol **392:** 614-629

19. Pilpa RM, Bayrhuber M, Marlett JM, Riek R, Young JA (2011) A receptor-based switch that regulates anthrax toxin pore formation. PLoS Pathog **7:** e1002354

20. Zhang S, Finkelstein A, Collier RJ (2004) Evidence that translocation of anthrax toxin's lethal factor is initiated by entry of its N terminus into the protective antigen channel. Proc Natl Acad Sci U S A **101:** 16756-16761

21. Zhang S, Udho E, Wu Z, Collier RJ, Finkelstein A (2004) Protein translocation through anthrax toxin channels formed in planar lipid bilayers. Biophys J **87:** 3842-3849

22. Abrami L, Lindsay M, Parton RG, Leppla SH, van der Goot FG (2004) Membrane insertion of anthrax protective antigen and cytoplasmic delivery of lethal factor occur at different stages of the endocytic pathway. J Cell Biol **166:** 645-651

23. Abrami L, Brandi L, Moayeri M, Brown MJ, Krantz BA, Leppla SH, van der Goot FG (2013) Hijacking Multivesicular Bodies Enables Long-Term and Exosome-Mediated Long-Distance Action of Anthrax Toxin. Cell Rep **27:** 986-996

24. Nablo BJ, Panchal RG, Bavari S, Nguyen TL, Gussio R, Ribot W, Friedlander A, Chabot D, Reiner JE, Robertson JW et al. (2013) Anthrax toxin-induced rupture of artificial lipid bilayer membranes. J Chem Phys **139:** 065101

25. Petosa C, Collier RJ, Klimpel KR, Leppla SH, Liddington RC (1997) Crystal structure of the anthrax toxin protective antigen. Nature **385:** 833-838

26. Jiang J, Pentelute BL, Collier RJ, Zhou ZH (2015) Atomic structure of anthrax protective antigen pore elucidates toxin translocation. Nature **521:** 545-549

27. Krantz BA, Finkelstein A, Collier RJ (2006) Protein translocation through the anthrax toxin transmembrane pore is driven by a proton gradient. J Mol Biol **355:** 968-979

28. Blaustein RO, Koehler TM, Collier RJ, Finkelstein A (1989) Anthrax toxin: channel-forming activity of protective antigen in planar phospholipid bilayers. Proc Natl Acad Sci U S A **86:** 2209-2213

29. Blaustein RO, Lea EJ, Finkelstein A (1990) Voltage-dependent block of anthrax toxin channels in planar phospholipid bilayer membranes by symmetric tetraalkylammonium ions. Single-channel analysis. J Gen Physiol **96:** 921-942

30. Krantz BA, Melnyk RA, Zhang S, Juris SJ, Lacy DB, Wu Z, Finkelstein A, Collier RJ (2005) A phenylalanine clamp catalyzes protein translocation through the anthrax toxin pore. Science **309:** 777-781

31. Nestorovich EM, Karginov VA, Berezhkovskii AM, Bezrukov SM (2010) Blockage of anthrax PA63 pore by a multicharged high-affinity toxin inhibitor. Biophys J **99:** 134-143

32. Das D, Krantz BA (2016) Peptide- and proton-driven allosteric clamps catalyze anthrax toxin translocation across membranes. Proc Natl Acad Sci U S A **113:** 9611-9616

33. Lee KI, Jo S, Rui H, Egwolf B, Roux B, Pastor RW, Im W (2012) Web interface for Brownian dynamics simulation of ion transport and its applications to beta-barrel pores. J Comput Chem **33:** 331-339

34. Orlik F, Schiffler B, Benz R (2005) Anthrax toxin protective antigen: inhibition of channel function by chloroquine and related compounds and study of binding kinetics using the current noise analysis. Biophys J **88:** 1715-1724

35. Montal M, Mueller P (1972) Formation of bimolecular membranes from lipid monolayers and a study of their electrical properties. Proc Natl Acad Sci U S A **69:** 3561-3566

36. Phillips DD, Fattah RJ, Crown D, Zhang Y, Liu S, Moayeri M, Fischer ER, Hansen BT, Ghirlando R, Nestorovich EM et al. (2013) Engineering anthrax toxin variants that exclusively form octamers and their application to targeting tumors. J Biol Chem **288:** 9058-9065

37. Yamini G, Nestorovich EM (2017) Relevance of the alternate conductance states of anthrax toxin channel. Proc Natl Acad Sci U S A **114:** E2545-E2546

38. Krantz BA (2017) Reply to Yamini and Nestorovich: Alternate clamped states of the anthrax toxin protective antigen channel. Proc Natl Acad Sci U S A **114:** E2547

39. Feld GK, Brown MJ, Krantz BA (2012) Ratcheting up protein translocation with anthrax toxin. Protein Sci **21:** 606

40. Krasilnikov OV, Sabirov RZ, Ternovsky VI, Merzliak PG, Muratkhodjaev JN (1992) A simple method for the determination of the pore radius of ion channels in planar lipid bilayer membranes. FEMS Microbiol Immunol **5:** 93-100

41. Nablo BJ, Halverson KM, Robertson JW, Nguyen TL, Panchal RG, Gussio R, Bavari S, Krasilnikov OV, Kasianowicz JJ (2008) Sizing the Bacillus anthracis PA63 channel with nonelectrolyte poly(ethylene glycols). Biophys J **95:** 1157-1164

42. Karginov VA, Nestorovich EM, Moayeri M, Leppla SH, Bezrukov SM (2005) Blocking anthrax lethal toxin at the protective antigen channel by using structure-inspired drug design. Proc Natl Acad Sci U S A **102:** 15075-15080

43. Bezrukov SM, Liu X, Karginov VA, Wein AN, Leppla SH, Popoff MR, Barth H, Nestorovich EM (2012) Interactions of High-Affinity Cationic Blockers with the Translocation Pores of B. anthracis, C. botulinum, and C. perfringens Binary Toxins. Biophys J **103:** 1208-1217

44. Bocquet L, Charlaix E (2010) Nanofluidics, from bulk to interfaces. Chem Soc Rev **39:** 1073-1095

45. Schoch RB, Han J, Renaud P (2008) Transport phenomena in nanofluidics. Rev Mod Phys **80:** 839-883

46. Aguilella-Arzo M, Aguilella VM, Eisenberg RS (2005) Computing numerically the access resistance of a pore. Eur Biophys J **34:** 314-322

47. Alcaraz A, López M, Queralt-Martín M, and Aguilella VM (2017) Ion transport in confined geometries below the nanoscale. Access resistance dominates protein channel conductance in diluted solutions. ACS Nano, in press.

48. Hall JE (1975) Access resistance of a small circular pore. J Gen Physiol **66:** 531-532

49. Dolinsky TJ, Nielsen JE, McCammon JA, Baker NA (2004) PDB2PQR: an automated pipeline for the setup of Poisson-Boltzmann electrostatics calculations. Nucleic Acids Res **32:** W665-7

50. Bezrukov SM, Vodyanoy I (1993) Probing alamethicin channels with water-soluble polymers. Effect on conductance of channel states. Biophys J **64:** 16-25

51. Levadny V, Aguilella VM, Belaya M (1998) Access resistance of a single conducting membrane channel. Biochim Biophys Acta **1368:** 338-342

52. Schiffmiller A, Anderson D, Finkelstein A (2015) Ion selectivity of the anthrax toxin channel and its effect on protein translocation. J Gen Physiol **146:** 183-192

53. Garcia-Gimenez E, Alcaraz A, Aguilella-Arzo M, Aguilella VM (2015) Selectivity of Protein Ion Channels and the Role of Buried Charges. Analytical Solutions, Numerical Calculations, and MD Simulations. J Phys Chem B **119:** 8475-8479

54. Liao SM, Du QS, Meng JZ, Pang ZW, Huang RB (2013) The multiple roles of histidine in protein interactions. Chem Cent J **7:** 44

55. Kullman L, Winterhalter M, Bezrukov SM (2002) Transport of maltodextrins through maltoporin: a single-channel study. Biophys J **82:** 803-812

56. Nestorovich EM, Danelon C, Winterhalter M, Bezrukov SM (2002) Designed to penetrate: time-resolved interaction of single antibiotic molecules with bacterial pores. Proc Natl Acad Sci U S A **99:** 9789-9794

Figures and Legends

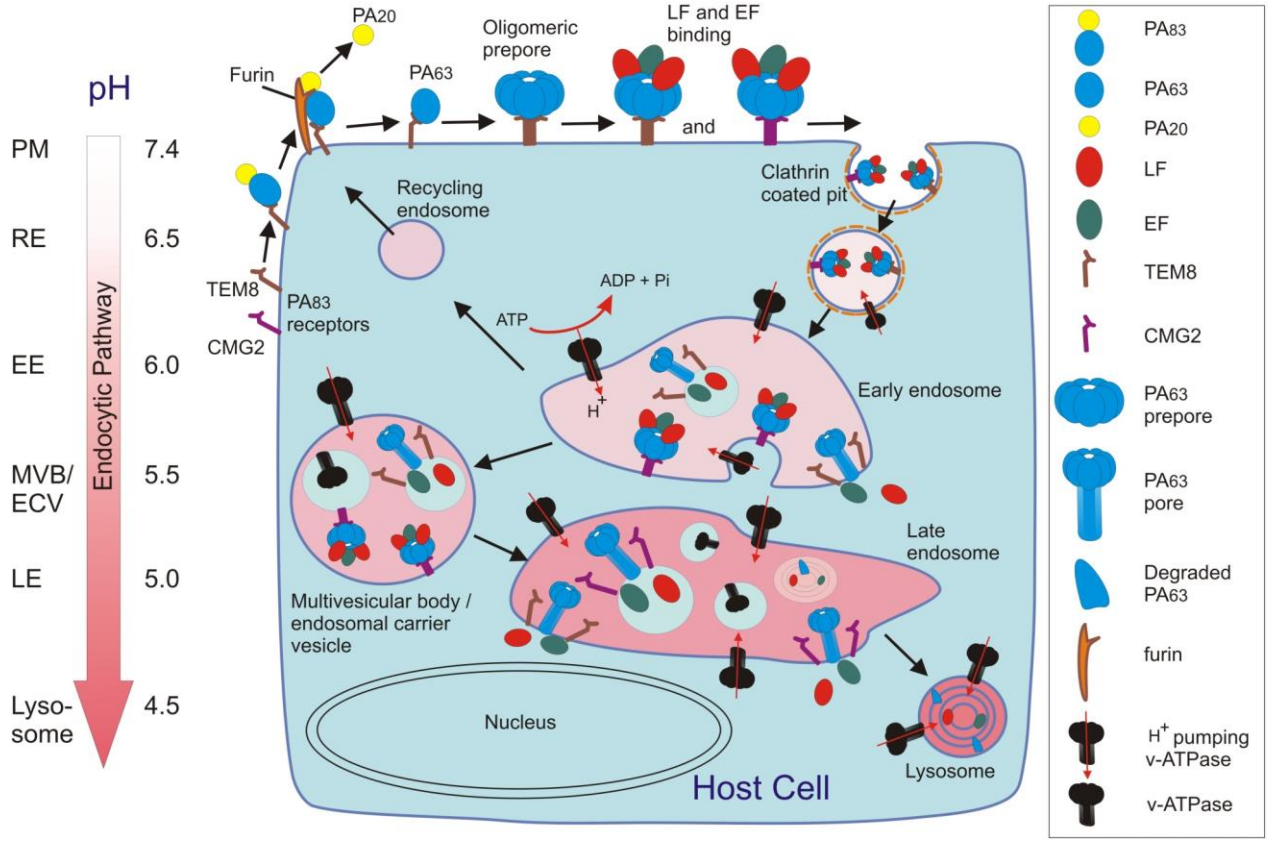

Figure 1. Schematic representation of the multistep anthrax toxin internalization process *(right)* and accompanying change in the pH environment *(left)*. First, PA_{83} binds to its cellular ANTXR1 (tumor endothelial marker-8 (TEM8)) [9] and ANTXR2 (capillary morphogenesis protein 2 (CMG2)) [10] receptors. After being cleaved to PA_{63} by furin-like proteases on the host cell surface and release of PA_{20} [16], it oligomerizes to form heptameric [25] and/or octameric prepores [18], which creates three (in heptamer) [17] or four (in octamer) [18] sites for the LF and/or EF binding. After receptor-mediated endocytosis [19], the anthrax toxin complexes are transited from the early to late endosomal multivesicular compartments, where they are exposed to the low endosomal pH. On uptake, the toxin complexes first encounter the early endosome pH environment (pH ~ 5.5 – 6.0) and then the late endosome pH environment (pH ~ 5.0 – 5.5). The endosomal acidification triggers substantial conformational changes of PA_{63} oligomers leading to their insertion into endosomal membranes and ion channel formation [25, 26]. The pH threshold for PA_{63} channel formation is different depending on which cellular receptor PA_{83} binds; pH 6.2 is sufficient to weaken the PA contact with TEM8, whereas pH 5.2 is required to weaken the stronger PA/CMG2 binding [11-13]. This indicates a possibility for the PA channel formation already at the early endosomal stage when the complex is bound to TEM8, however the lower late endosomal pH is required when the complex is bound to CMG2 [14, 15]. The formed channel is then believed to work as an effective translocase, capable of unfolding and translocating LF and EF into the cytosol under a pH gradient across the late endosomal limiting membrane [20, 21]. Apart from translocating LF and EF through the endosomal limiting membrane, PA/LF and PA/EF complexes also preferentially insert into endosomal intraluminal vesicle (ILV) membranes [22, 23].

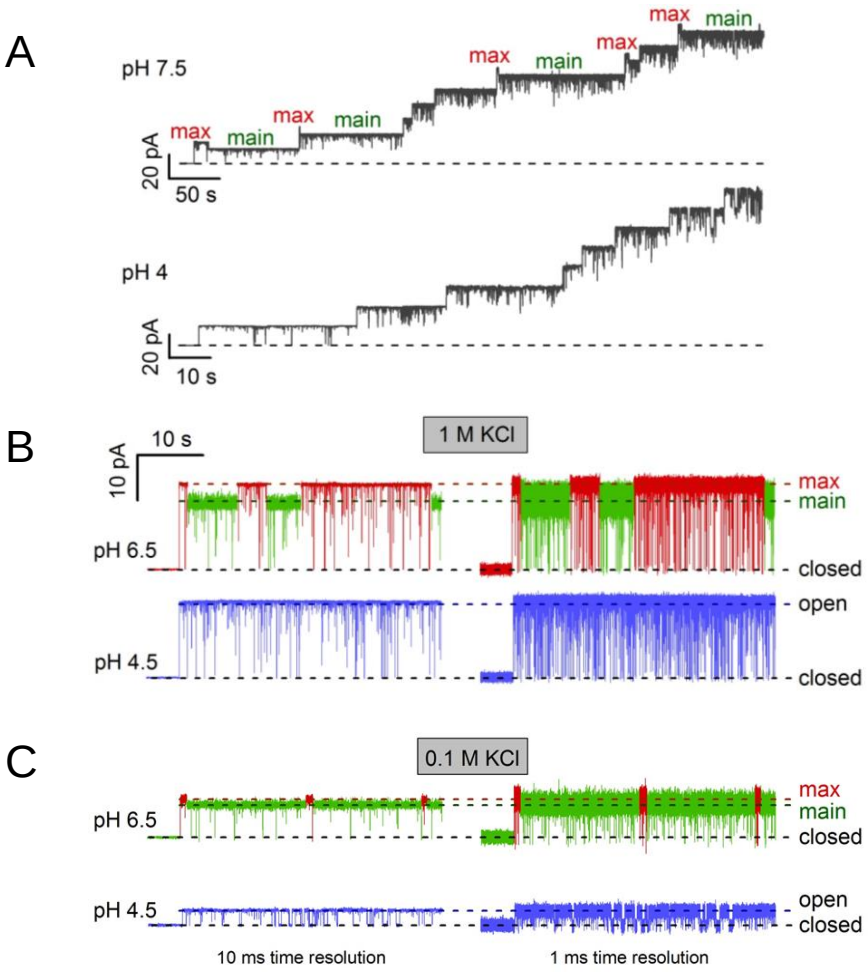

Figure 2. Influence of pH on the two conductance states of the open PA_{63} channel. *(A)* PA_{63} channel insertion recordings taken at pH 7.5 *(top)* and pH 4 *(bottom)* under 100 mV *cis*-positive applied voltage in 1 M KCl. 50-ms averaging interval was used. Note that at pH 7.5, 5 out of 9 single channels first insert in the maximum conductance state, quickly changing to the main conductance state. *(B and C)* Single PA_{63} channel recordings taken in 1 M *(B)* and 0.1 M KCl *(C)* solutions at pH 6.5 (*top*) and pH 4.5 (*bottom*) and shown using 10-ms (*left*) and 1-ms (*right*) averaging interval. Note the presence of the maximum (*red*) and main (*green*) conductance states at pH 6.5, the only conductance state (*violet*) at pH 4.5, and the difference at the current noise level when in the maximum and main conductance states.

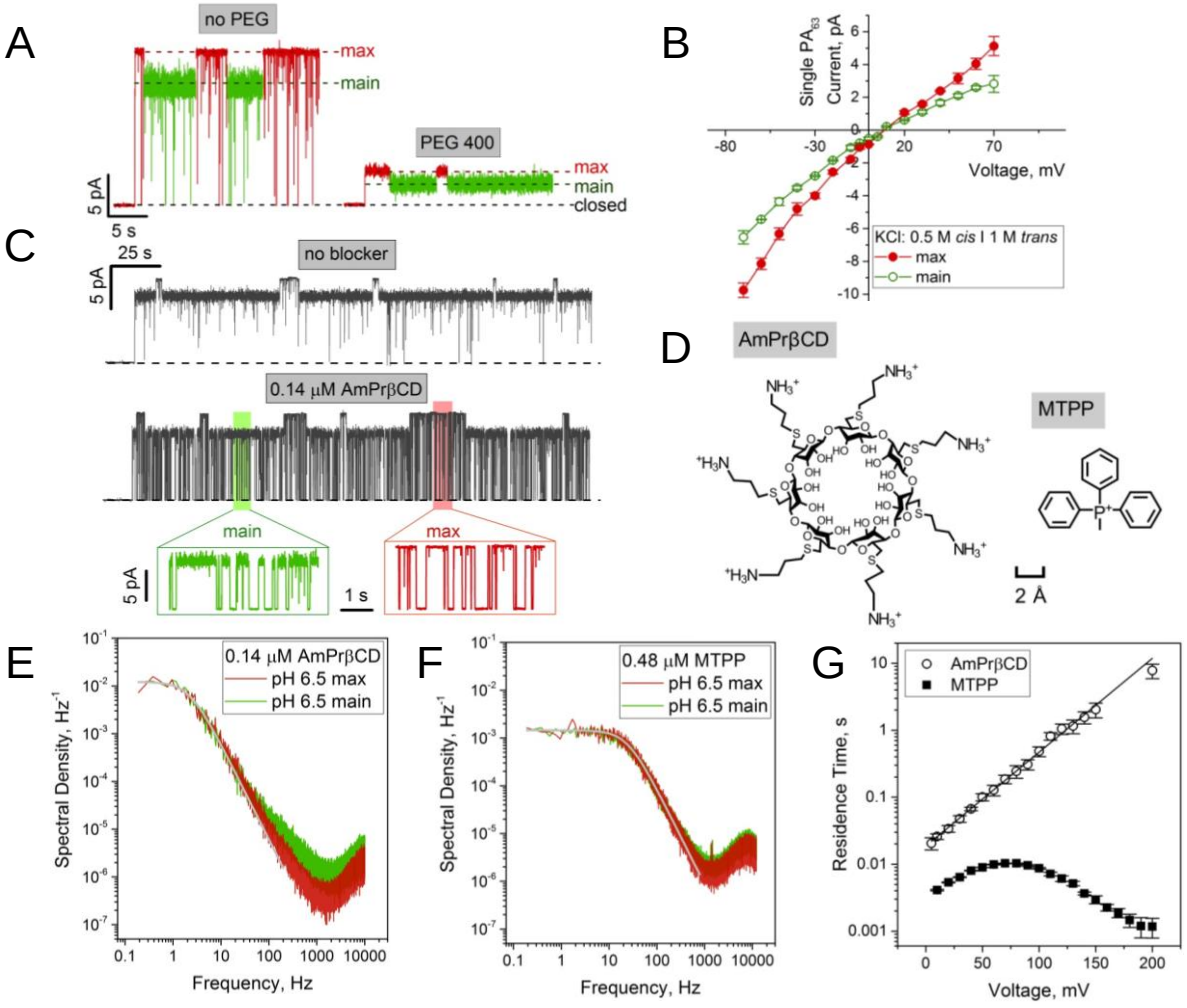

Figure 3. Characterization of the maximum and main conductance states of PA_{63}. *(A)* Two states of the open PA_{63} single channel examined in PEG free (*left*) and 1.2% (w/w) PEG 400 containing (*right*) 1 M KCl solutions at pH 6.5. The applied potential was 100 mV. *(B)* Ion current *versus* voltage relationship separately taken for the single PA_{63} channels when in the maximum (*red filled circles*) and main (*green open circles*) conductance states using 0.5 M *cis* | 1 M *trans* KCl gradient at pH 6.5. Note that the reversal potentials in both states are very similar: 9.1 ± 0.5 mV in the maximum conductance states and 8.6 ± 0.4 mV in the main conductance state. The data represent averaging over three single-channel recordings. *(C)* AmPrβCD channel inhibitor blocks PA_{63} both when the channel is in the main and maximum conductance states. In the absence of AmPrβCD *(top)*, fast flickering between open and closed states was mainly removed by averaging over a time interval of 50 ms. In the presence of AmPrβCD, the channel gets spontaneously blocked *(bottom)* both when it is in the main *(green insert)* and maximum *(red insert)* conductance states. Probabilities of finding the channel in the blocked state were similar for the main ($p_{bl} = 0.234$) and maximum states ($p_{bl} = 0.236$). The dashed lines represent zero current levels. The inserts were averaged over 10 ms. The data are obtained under 50 mV applied voltage in 1 M KCl at pH 6.5. *(D)* Multivalent AmPrβCD *(left)* and small-molecule MTPP (*right*) cationic blockers of PA_{63} channel. Note that the 2 Å scale bar provides only an approximate molecule dimension due to conformational flexibility of the compounds and omitted hydrogen atoms. The images were created using chemical drawing software ChemDoodle 8.1.0, iChemLabs, LLC. *(E)* Power spectral densities of AmPrβCD-induced PA_{63} current fluctuations in the main *(green spectrum)* and maximum *(red spectrum)* conductance states at frequencies <100 Hz can be fitted by a single Lorentzian *(solid line, shown for the maximum conductance state)*. The increase in the current spectral density signal on the main state spectrum observed at high frequencies (> 100 Hz) is related to increase in the current fluctuation intensity, as described separately (see Figs. 2B, 4B and the related discussion). *(F)* Power spectral

density of MTPP-induced PA_{63} current fluctuations in the main *(green spectrum)* and maximum *(red spectrum)* conductance states are fitted by a single Lorentzian (solid line, shown for the maximum conductance state). The data are recorded under 50 mV applied voltage in 1 M KCl at pH 6.5. In *(E)* and *(F)*, the spectra were normalized by dividing the current power spectral density by the square of the mean current, I_{main}^2 or I_{max}^2, to account for the difference in the two state conductances. *(G)* Residence times of AmPrβCD (open squares) and MTPP (filled circles) binding to PA_{63}, as functions of voltage (1 M KCl, pH 6.5), show different patterns of their interaction with the pore. While the AmPrβCD blockage times are practically exponential in the voltage applied to the membrane *(a solid line)*, the MTPP blockage time, first increasing with voltage, shows a subsequent decrease, earlier described for maltodextrin [55] and ampicillin [56] molecules which are evolved to bind and translocate through bacterial maltoporin and OmpF porin respectively. The residence times were calculated by spectral analysis of current fluctuations as described previously [42]. Both maximum and main conductance states were used for the analysis. In *(B)* and *(G)*, the errors bars are standard deviations.

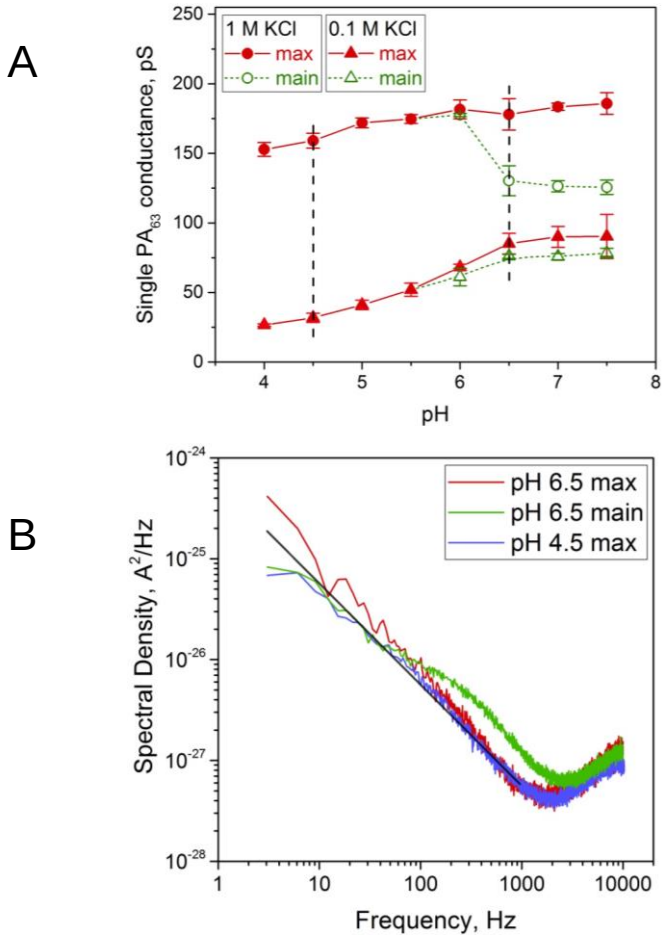

Figure 4. *(A)* Single PA_{63} channel maximum state current decreases when bathing solution pH is lowered from 7.5 to 4, both in 1 M KCl (*filled red circles*) and 0.1 M KCl (*filled red triangles*) solutions. The effect is more pronounced in 0.1 M KCl compared to 1 M KCl. Thus, with pH decrease from 7.5 to 4, the current is reduced by ~3.4 times and ~1.2 times, respectively in 0.1 M and 1 M KCl solutions. At high pH values, the main conductance states were frequently detected (*open green symbols connected by the dashed lines*). The measurements were performed at 100 mV applied voltage. The error bars represent standard deviations. The maximum and main conductance states, even if detected for the same single channel, were counted as separate channels, whereas the small conductance change-overs between these two states (seen as transition steps between two dashed lines in Fig. 2B and C) were not counted as separate events. *(B)* Spectral density analysis of the current fluctuation through single PA_{63} channel in pH 6.5 and pH 4.5 solutions. At pH 6.5, current fluctuations both when in the maximum (*red spectrum*) and main (*green spectrum*) states are analyzed. At pH 4.5 (*violet spectrum*), the current spectra density changes linearly with frequency at a wide 3 - 1000 Hz range of frequencies (slope ≈ -1.0), showing typical characteristics of the so-called *1/f* process. In the main conductance state at pH 6.5, the spectrum (*green*) is similar; however we observed an additional high-frequency component that corresponds to the "noisy" sub-state of the channel (*marked in green in Figs. 2B, 2C and 3A*). At pH 6.5, spectral density analysis of the completely open state of the channel, collected from several opening events combined into a single fragment (*red spectrum*), showed an ideal *1/f* type of behavior (slope ≈ -1.1), similar to the one observed at pH 4.5.

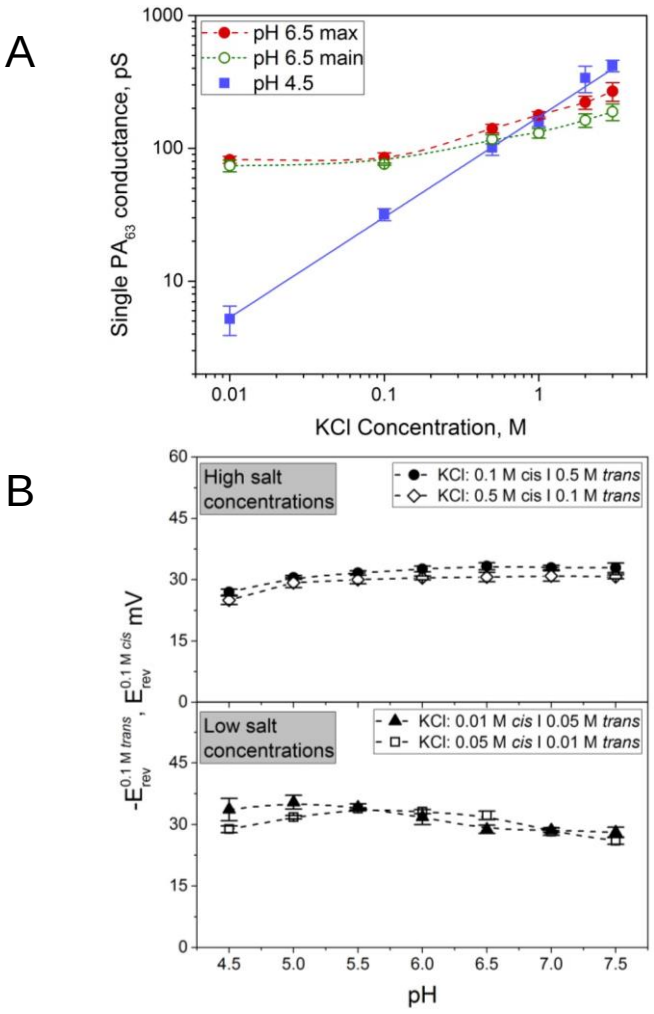

Figure 5. *(A)* Single PA_{63} channel current dependence on bathing KCl concentration is different when measured in neutral and acidic solutions. While at pH 6.5 we observed a weak dependence of PA_{63} conductance on solution concentration, both in the maximum (*red filled circles*) and main (*green open circles*) conductance states, at pH 4.5 *(violet squares)* channel conductance changes linearly with the bulk solution concentration. *(B)* Dependence of the anthrax toxin channel reversal potential on solution pH. *Top:* The measurements are taken using 0.1 M KCl and 0.5 M KCl, in *cis* and *trans* compartments of the bilayer chamber correspondingly (*filled circles*) and then the KCl gradient was reversed *(open diamonds). Bottom*: PA_{63} selectivity measurements taken using 0.01 M *cis* and 0.05 M *trans* KCl solutions (*filled triangles*) and the reversed gradients (*open squares*). To make the comparison easier, the data for the inverted gradient are plotted as $-E_{rev}$. Both in *(A)* and *(B)*, the error bars represent standard deviations.